ARTICLE IN PRESS

Precision Engineering xxx (xxxx) xxx–xxx

Contents lists available at ScienceDirect

Precision Engineering

journal homepage: www.elsevier.com/locate/precision

A tip-based metrology framework for real-time process feedback of roll-to-roll fabricated nanopatterned structures

Liam G. Connolly, Tsung-Fu Yao, Andrew Chang, Michael Cullinan*

Walker Department of Mechanical Engineering, The University of Texas at Austin, Austin, TX, USA

ARTICLE INFO

Keywords:
Roll-to-Roll
Metrology
Flexible electronics
In-line process control
Scanning probe microscopy
Atomic force microscopy
Flexure mechanism
Nanopositioner

ABSTRACT

This paper presents the development of a metrology framework and proof-of-concept tool to perform direct, nanometer-scale topography measurements for real-time process control in the roll-to-roll manufacturing of nanopatterened materials, films, and flexible electronic devices. The system leverages a uniquely compact single chip atomic force microscope (sc-AFM) based on a micro-electromechanical system (MEMS) architecture with custom approach mechanism positioned on a gantry which is actuated by two vertical, double parallelogram flexure mechanism guided two-axis nanopositioners. This probe is situated over a stainless-steel, air bearing supported idler roller and its position dynamically compensated for curvature, eccentricity and surface topography of the roller during web movement through the system from an offline map. The proof-of-concept tool performs a single, $400\,\mu m^2$, non-contact tapping mode scan with nm height resolution on a flexible, $150\,\mu m \times 350\,mm$ polycarbonate substrate every 60 s in a step-and-scan fashion where web movement occurs during each step. The performance of the sc-AFM gantry nanopositioning system is evaluated and a representative nanofeatured flexible material, the wing of a Queen Butterfly, is used as a test artifact to demonstrate the efficacy of the nanometrology data acquired. This capability represents a wholly new method for in-line metrology in roll-to-roll nanomanufacturing.

1. Introduction

While the falling cost of electronic devices has driven global proliferation to great benefit, over half the world's population still has no access to the internet – primarily due to high device costs [1]. Further, the same barrier is found with many high-efficiency energy storage and conversion devices such as high energy-density batteries, solar cells, supercapacitors, and fuel cells [2]. A large part of the cost for many of these devices comes from processing and fabricating the requisite nanofeatured materials and systems to achieve optimal performance. The promise of roll-to-roll (R2R) manufactured products is to bring an exceptional combination of large, continuous processing area, and thus low unit cost, and extremely desirable mechanical properties to these markets. Yet, the mass-fabrication systems and methodologies needed to produce devices at scale, and lower the barriers to entry for these wide-reaching sectors, are lagging far behind potential product development. Achieving feasible production of these flexible devices has proven difficult and time consuming, especially when moving beyond lab-scale fabrication [3–6].

The most prominent barrier to the development of new volume R2R nanomanufacturing techniques or R2R fabricated devices, when polled by the US National Institute of Standards and Technology (NIST), is the difficulty in implementing viable real-time, in-line process feedback for devices which require nanoscale features for optimal performance. This is exceedingly important for R2R applications as it is often very costly for a manufacturer when a process goes out of control and this process shift isn't detected until an entire roll of product is fabricated and functional testing of the devices or materials on the substrate can be measured with an out-of-line sample. This troubling situation can result in large amounts of processed material, produced to a sub-standard grade, which needs to be scrapped at a potentially enormous loss. The large area processing of these R2R techniques will only be advantageous from a cost perspective if scrap rates can be kept low – necessitating a true nondestructive, in-line metrological methodology for R2R nanomanufacturing [7,8]. Moreover, such a system could benefit not only mass production applications, but also new product or process development, as a higher throughput of metrology data during the research and development phases of new devices can significantly aid in lowering the overall development time required to bring a new R2R process to maturity.

* Corresponding author.
E-mail address: Michael.Cullinan@austin.utexas.edu (M. Cullinan).

https://doi.org/10.1016/j.precisioneng.2019.04.001
Received 4 December 2018; Received in revised form 5 March 2019; Accepted 2 April 2019
0141-6359/ © 2019 Elsevier Inc. All rights reserved.

Please cite this article as: Liam G. Connolly, et al., Precision Engineering, https://doi.org/10.1016/j.precisioneng.2019.04.001

ARTICLE IN PRESS

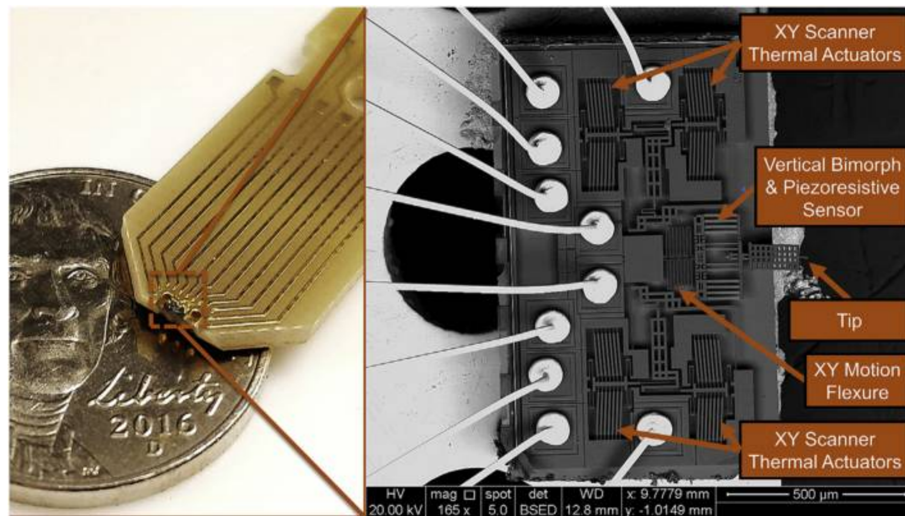

Fig. 1. Photo of sc-AFM and wire-bond PCB on a US Nickel and SEM Image showing sc-AFM major subsystems.

1.1. Current metrology methods

The field of metrology for R2R production lines focuses on the non-contact, non-destructive evaluation of masks, templates, thin-film topography, patterned intermediate steps, and final products. Current metrology systems for R2R applications have followed the example set in traditional semiconductor manufacturing, with optical methods dominating in-line inspection and slower, higher resolution methods such as critical dimension scanning electron microscopy (CD-SEM) or traditional scanning probe microscopy (SPM) used for more detailed inspection of tooling, nanofeatured masks, or selective out-of-line samples. Although exact numbers are a closely held trade secret, it is believed that sampling in a typical modern fab would be on the order of 1 out of every 50 wafers pulled out-of-line for CD-SEM review, which itself can take over 700 h depending on area of the wafer scanned and to what resolution [9]. While there have been recent advances in using optical methods such as scatterometry, diffractometry, ellipsometry, interferometry, 1D profilometry, thermography and other laser light microscopy techniques to measure materials with sub-wavelength features such as periodically patterned films and hierarchical materials, real-time and in-line feedback of directly inspected structures on tooling, intermediate process steps, or products with critical dimensions beyond the diffraction limit of optical techniques is necessary to fully realize the cost benefit of R2R manufacturing [4,8,10–21]. The issue arises when optical methods for direct inspection fail to resolve the individual critical dimension levels desired for maximal performance and packaging of this new class of R2R manufactured products due to diffraction limits, especially when measurement of specific features at particular locations of interest is required as opposed to collections of features, like in most indirect optical based techniques. This capability of direct feature measurement is unique to SPM and e-beam based inspection. However, e-beam inspection techniques are typically much too slow, and vacuum requirements much too strict, for any sort of effective in-line operation in the R2R environment where high processing speeds are necessary to achieve desired unit-cost goals. Thus, in an ideal R2R nanofabrication process, optical techniques can provide feedback on any large defects and general fabrication quality for hierarchical or repeated structures in parallel with a system or device to conduct direct real-time sampling of CD features of interest such as line edge roughness, aspect ratio, profile geometry, pitch, and thickness – all in-line with the R2R process.

In order to provide the true real-time feedback of individual, nanoscale features, required, a series of barriers must be overcome. Any proposed system must be able to function nominally in the relatively noisy environment of a R2R manufacturing line, achieve significantly higher throughput than existing nanoscale techniques like multi-hour CD-SEM, not contribute significantly to the overall cost of R2R manufacturing, and most importantly, do so in a non-contact fashion in-line with existing nanofabrication processes. A new framework for high-speed, in-line R2R inspection of nanoscale features is required to effectively pursue the fabrication techniques and flexible electronic devices of tomorrow. The aim of this work is to develop this metrology framework and present a proof-of-concept system which demonstrates this methodology.

1.2. sc-AFM operation and advantages

The recently developed single chip atomic force microscope (sc-AFM, Integrate Circuit Scanning Probe Instruments [ICSPI] Corp.) represents a huge leap forward in both compactness of design and price point compared to traditional table-top scanning probe systems. Most traditional AFM tools use an expensive and bulky laser-based measurement system to sense tip deflection and short range, high accuracy and high cost piezo-based stages to scan across a substrate. This methodology, while able to resolve 5 and 7 nm node sized features, is bulky, costly, and ill-suited for in-line metrology applications [22]. The sc-AFM, shown in Fig. 1, consists of integrated X and Y scanning thermal actuators and flexure bearings and a vertical bimorph and piezoresistive cantilever sensor for sensing and actuation of a cantilevered tip. Unlike traditional AFMs, the micro-scale motion mechanisms of the sc-AFM and small moving masses lead to high resonance frequency ($>$ 9 kHz), and thus very fast scanning speeds are possible while also attaining good base vibration rejection and minimizing the effect of errors such as thermal drift. The maximum and minimum scanning field of view is 20 μm × 20 μm and 1 μm × 1 μm respectively, and maximum active tip actuation range is 10 μm. The scan speed of the sc-AFM is 0.15 s/line and, while dynamic cantilever RMS noise floor is $<$ 1 nm, the minimum feature height for accurate topography scanning is 10 nm. The aluminum oxide tip is guaranteed to be less than 80 nm in radius. Further, the footprint of the device is extremely small, a multiple order-of-magnitude reduction when compared to traditional table top AFMs. This compact design, with less than 0.25 mm^3 volume, lends itself extremely well to in-line applications where space is at a premium, and all that is required in terms of connections is a 12-pin ribbon cable to a remote controller – driver. The sc-AFM is also designed for fully non-contact, tapping-mode scans which can measure nm-level surface topology and is preferred for applications where non-destructive evaluation is required. This mode of operation also

significantly limits operation costs, with no visible tip wear seen in sc-AFMs after over 10,000 individual scans [23]. This collection of features, along with its extremely low price, $250 per device, makes the sc-AFM a perfect candidate to be applied in-line with R2R nanofabrication processes [24–28].

1.3. In-line system operational methodology

The compact nature of these sc-AFMs also allow for the unique ability to package a multiplicity of probes all scanning a single web in one tool – thus enabling proportional expansion of the scanning area of the system well beyond traditional single-cantilever AFM measurement tools. This is critical for any R2R metrology tool to greatly increase the overall throughput and modularity of direct, nanometer-scale measurement [24,25,29]. The metrology system is designed to operate at a speed commensurate with what is required for in-line process control of structures fabricated with step-and-repeat R2R nanopatterning methods. These typically involve stepper-based or serial write processes such as mask-less (digital mirror array based) photolithography [30], traditional R2R photolithography [31], and stepped mechanical imprint techniques to produce both final products and master template "shims" for roller-based continuous nanofabrication processes like ultraviolet (UV) nanoimprint lithograph (NIL) [32–34]. One extremely promising such stepped R2R nanofabrication technique is Jet-and-Flash Nanoimprint Lithography (JFIL) [35–37]. In this instance, a roughly 60 s step-and-repeat cycle time is standard for commercial JFIL process developed from more traditional wafer-based JFIL tools (e.g. roll-to-"plate") [38,39]. As the proof-of-concept tool is intended to function in-line with such a JFIL system (LithoFlex 100), the proposed tool thusly operates with a step-and-scan principle to acquire nanometrology data from fabricated structures.

Positioning of the AFM probe is split into three coupled sub-systems during metrology operations. First, the gantry structure above the web to which the AFM is mounted is positioned in both the vertical and lateral (machine) directions to within 200 μm of the web by means of dual-monolith flexure bearing based positioners with feedforward control. The fine approach mechanism then brings the sc-AFM within 10 μm of the substrate in closed loop operation using the piezoresistive cantilever sensor on the sc-AFM as approach feedback. Once at optimal scanning height, the fine approach system is held at a constant open-loop height while the discrete sc-AFM controller begins actuating the measurement tip to perform the scan. After scanning is complete, the sc-AFM is returned to a safe height to prevent any destructive tip-sample interference. It is kept roughly 150 μm from the substrate during web travel using an offline mapping of the metrology roller topography to compensate for changes in height as the metrology idler roller rotates. Once the next desired "hotspot" for process control reaches the plane of the AFM tip, web movement is halted, and the AFM is once again approached to within 10 μm of the web and scans another 400 μm^2 imaging area. This workflow is also shown in Fig. 2.

Based on this mode of operation and system flow, specific design requirements for the nanometrology proof-of-concept tool are that proposed system must:

(1) Accurately position AFM probe in vertical and machine directions
  a. Position the sc-AFM with nm-scale precision
  b. Minimize noise floor (sub 10 nm 1-σ deviation)
  c. Accept large moving masses (> 3 kg)
(2) Prevent tip crashing under all operational circumstances
  a. Achieve good disturbance rejection in the 0–20 Hz range (> 20 Hz first resonance)
  b. Reach a mm retract range for sc-AFM probe
(3) Achieve high throughput (60 s Cycle Time)
  a. Minimize sc-AFM approach and retract motion times
(4) Provide constant web tension during static sc-AFM scans
  a. Implement a calibrated web tension control

A system embodying these requirements is shown as a render in Fig. 3. The design consists of two vertical nanopositioner stages rigidly connected by a gantry which holds the sc-AFM probe with its fine approach mechanism and voice coil actuator. This gantry is positioned over a flexible web which travels over an air bearing supported, live shaft idler roller with web travel regulated by cantilevered unwind and rewind stands.

2. System design and analysis

2.1. Web handling

The web handling subsystem design was primarily driven by the constraint of not damaging any sensitive or uncured patterns on the top-side of the substrate. In larger, full-scale systems this no-top-side-contact requirement can be mitigated by the use of protective films on top of fabricated structures, but this requires extra complexity in de-leaving and interleaving the film upon unwinding and rewinding respectively [40,41]. By choosing to avoid web top-side contact, the design for this subsystem and number of rollers can be simplified, but this non-contact requirement also rules out any classical R2R tension control methods such as spring-loaded dancer rollers or load-cell roller based tension feedback control [42,43]. Moreover, as the tool was intended to be widely adaptable to a variety of R2R processes, regardless of where precisely in the R2R nanofabrication line it will operate, the web handling sub-system is designed to be an analog for real-time process feedback at various different stages of the manufacturing process.

The web handling system consists of three rollers: an unwind stand, an idler metrology roller, and a rewind stand as shown in Fig. 4. Each winding stand in the subsystem consists of an extruded aluminum structure rigidly bolted to an air isolated optical table (Newport ST2) and two, four-bolt flange-type self-aligning spherical roller bearings

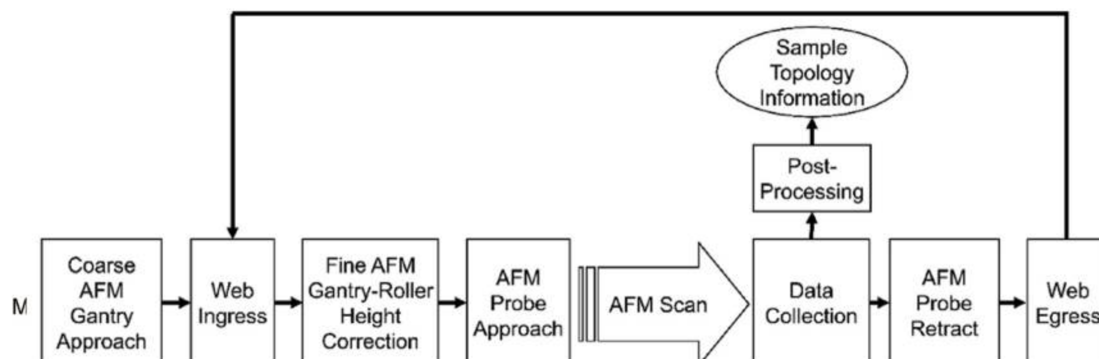

Fig. 2. System operational flow.

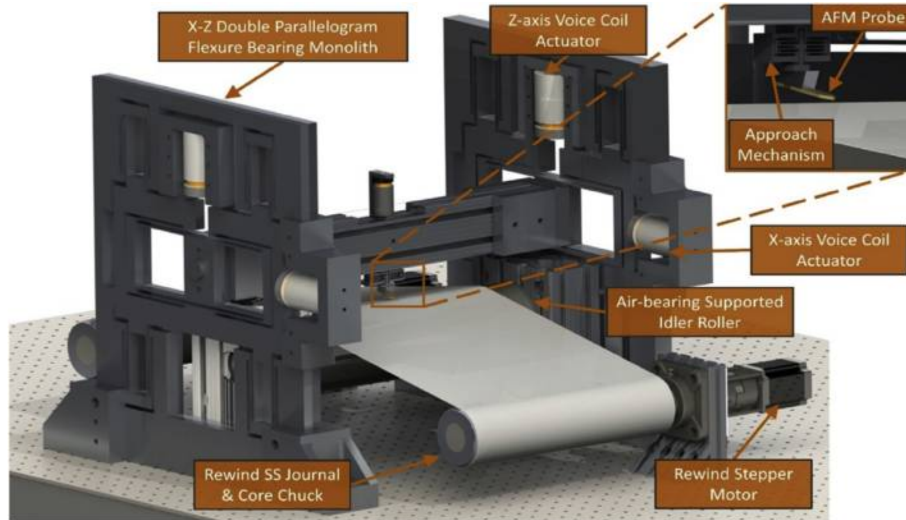

Fig. 3. Proof-of-concept system CAD overview.

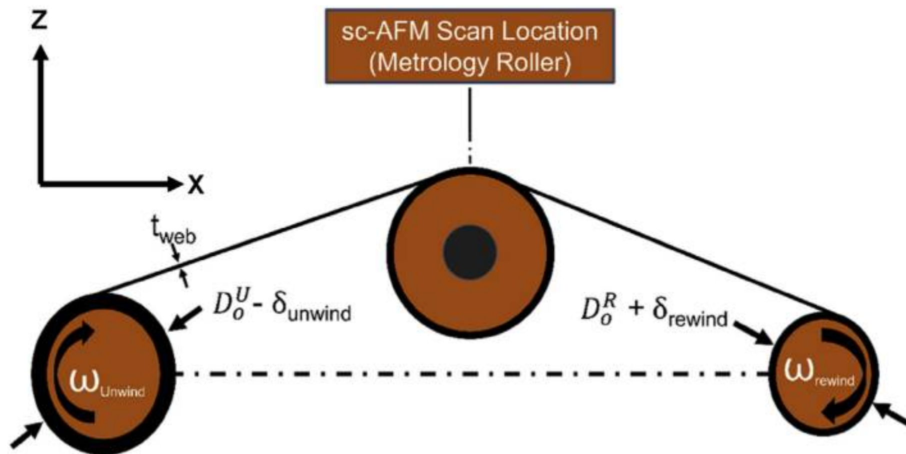

Fig. 4. Geometric layout of web handling sub-system.

Table 1
DPFM design parameters.

Parameter	Value	Parameter	Value
L_X	80 mm	k_x	46.1 N/mm
L_Z	95 mm		
B_X	25.4 mm	k_z	32.7 N/mm
B_Z	25.4 mm		
H_X	1.5 mm		
H_Z	2 mm	Maximum Range (X)	2.8 mm
FOS	3	Maximum Range (Z)	4.18 mm

(UCF208-24) on either side of the structure together support a turned 304-series alloy stainless steel journal. Rolls of nanopatterened, 150 µm thick (t_{web}) polycarbonate film 300 mm wide are held to the journal through a standard 3-inch core diameter air-bladder expansion chuck which is attached to the journal with a c-style clamp (PARA Co.). This cantilevered layout with air chucks allows for quick changing of the rolls of material used in the system for testing and the modulation of the speed and torque applied by these unwind and rewind stands controls material flow and web tension of the system.

2.1.1. Unwind tension control

To control the unwind tension of the web handling sub-system, a three-phase, brushless AC-commutated servo motor with integrated angular resolver and a 5 kHz high-speed servo controller-driver are utilized for the unwind motor system (Pacific Scientific, R33HENC-HS-NS-NV-00, Parker Hannifin, APEX 6151). The static motor torque is controlled as a percentage of maximum possible servo motor torque by the controller-driver. This duty cycle setting is calibrated to a static torque transducer under torque-stall conditions with 5.6 mN accuracy to ensure proper motor output torque of 10 N for web tensioning during sc-AFM scans (Transducer Techniques TRT-200). For dynamic torque modulation during web movement, the servo controller is operated in torque control mode as an electronic brake. To properly modulate output torque as roller diameter changes dynamically with unwinding, a triangulating laser distance sensor is used to continuously monitor the absolute unwind roll diameter, ($D_o^U - \delta_{Unwind}$), with 10 µm accuracy (Baumer OADM 13i64) and this data is sent to the servo controller where it is utilized as feedback to modulate the motor torque and provide a constant tension to the web during movement using equation (1) where F, τ, and D correspond to web tension, motor torque, and roll diameter respectively.

$$F_{tension} = \tau * (D_o^U - \delta_{Unwind}) \tag{1}$$

2.1.2. Rewind position and velocity control

The rewind journal is actuated by standard NEMA 23 stepper motor (Anaheim Automation, 23W209S-LW8) driving the journal via a timing belt and pulley. The motor is driven by an open source, Arduino based

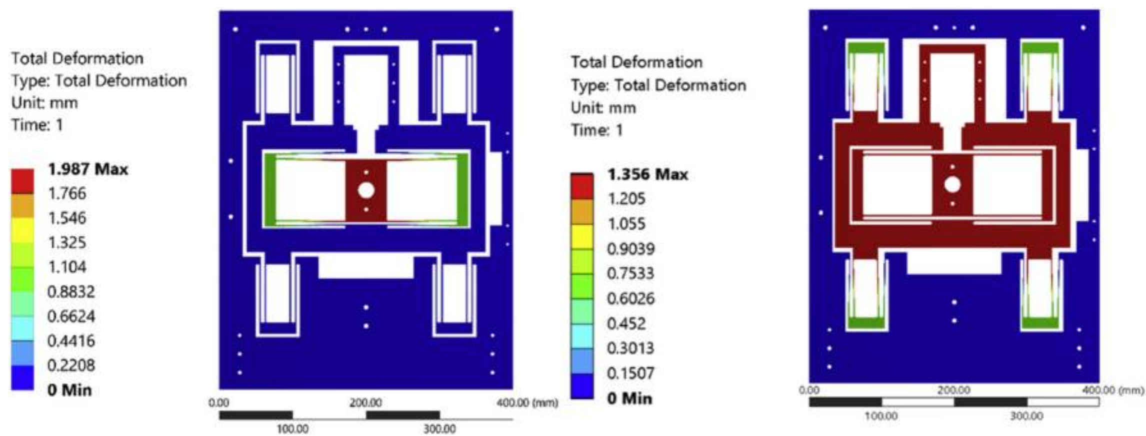

Fig. 5. DPFM Z (left) and X (right) axis movement to 68 N maximum unidirectional voice coil actuator force.

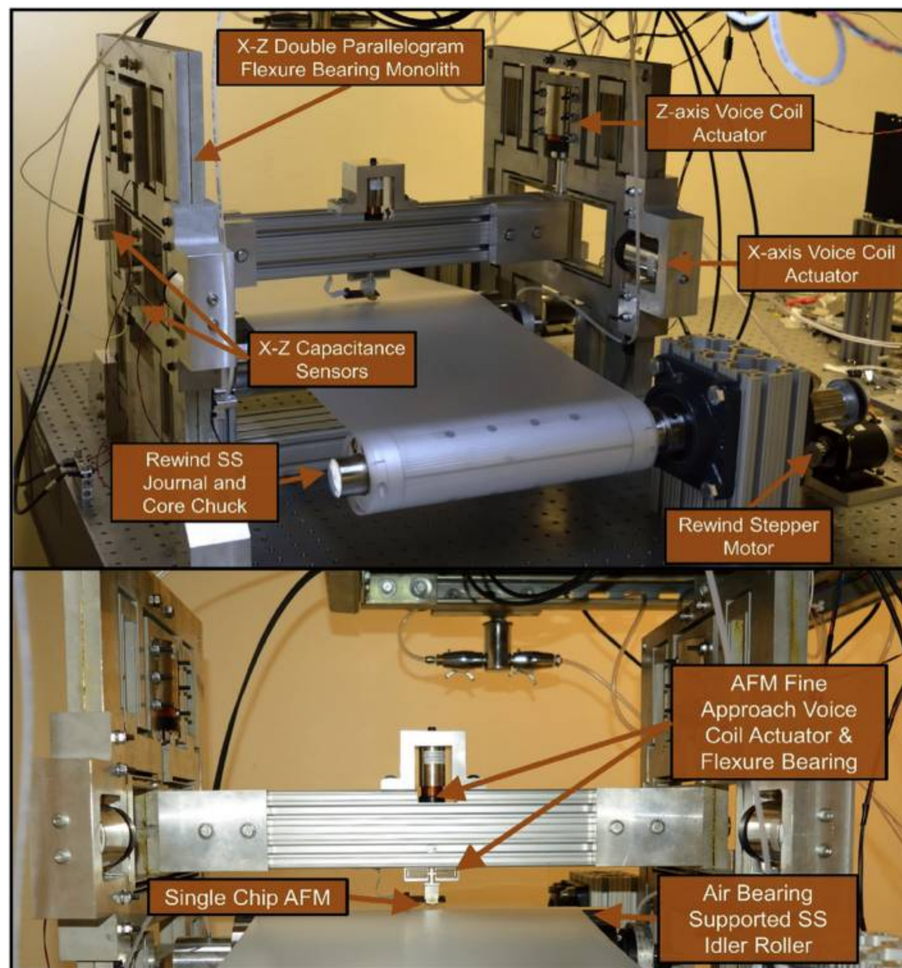

Fig. 6. Nanometrology proof-of-concept prototype system overview.

open loop, micro-stepping controller (Syntheos, grbl). The absolute (multi-turn) rotational position of this motor since startup, δ_R, in addition to an off-line initial roll diameter, D_o^R, is used to actuate the rewind roller in order to produce a constant web velocity.

2.1.3. Metrology roller

The roller on which the sc-AFM scans take place must remain stable under static and dynamic conditions so as to not adversely affect the accuracy of metrology data taken with the sc-AFM. Rotary air bearings were chosen over traditional spherical or tapered roller bearings for their ultra-low friction, high stability, vibration isolating properties, and low total runout error in order to achieve this challenging constraint during web motion, and thus roller rotation. Polished 304 stainless steel (R_a 0.01 μm) was chosen as the material for the roller due to its good thermal and chemical stability, cleanroom compatibility, stiffness, and low wear as a bearing surface. For feedback of roller position, an angular, 12-bit hall effect encoder is attached via a flexible coupling to the metrology roller (MEGATRON Elektronik MAB22A).

ARTICLE IN PRESS

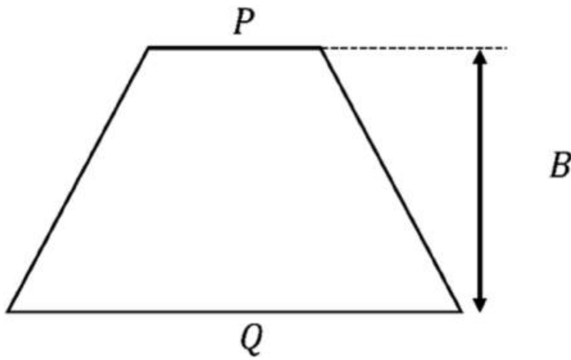

Fig. 7. Kerf cross section diagram.

2.2. Gantry nanopositioner

2.2.1. Flexure design overview

The flexure stages utilized for this proof-of-concept tool have to meet a series of specifications to optimize performance of the positioning sub-system. The gantry to which the sc-AFM approach system and probe are mounted must be rigid enough to not contribute significant error to the nanoscale measurements of the sc-AFM, thus necessitating a high moving mass to achieve this gantry stiffness. Further, given that the gantry will be suspended by the nanopositioning system, a high out-of-plane and torsional stiffness, and good resistance to any potential beam buckling is necessary. Moreover, in order to ensure the accuracy of the in-line sc-AFM scans, the nanopositioner system must achieve nm-scale uncertainty in position, a high bandwidth for disturbance rejection during delicate sc-AFM scanning processes and high-speed operation, and a large enough range for proper sc-AFM sample separation during web movement between scans. This range is also necessary to allow for easy replacement of any broken sc-AFM probes.

These requirements on range, resolution, carrying capacity (moving mass), and bandwidth place the proposed double parallelogram flexure mechanism (DPFM) based nanopositioner in an ill-explored area in current literature, situated between ultra-stiff, high bandwidth (200 + Hz) piezo actuated positioners and low stiffness, lower bandwidth, long-range voice coil actuated flexure positioners which can have thin enough flexure beams to compromise out of plane and transverse (e.g. orthogonal to the mechanism direction) stiffness for larger moving masses and vertical mechanism orientations. Further, low frequency vibrations in the 0–20 Hz range are common to large scale R2R manufacturing. Most air-isolation tables, like that upon which the proof-of-concept tool is built, are ill-suited to attenuating low frequency building vibrations below 20 Hz, so a first resonant mode above 20 Hz was desired for each flexure axis as the higher the first resonance mode, the less susceptible the mechanism will be to ground vibrations, thus lowering the overall noise floor. The nanopositioners are also designed to accept a moving mass roughly 2 kg heavier than currently implemented for planed future, multi-probe measurements where the additional approach voice coil actuators will add significant mass. Lastly, in order to minimize costs for production of the large DPFM monoliths, all design parameters are restricted by the limited repeatability, absolute accuracy, and kerf control for higher thickness cuts using an abrasive water jet cutting (AWJC) processes to fabricate the flexure mechanisms. 6061-T651 aluminum was chosen for its

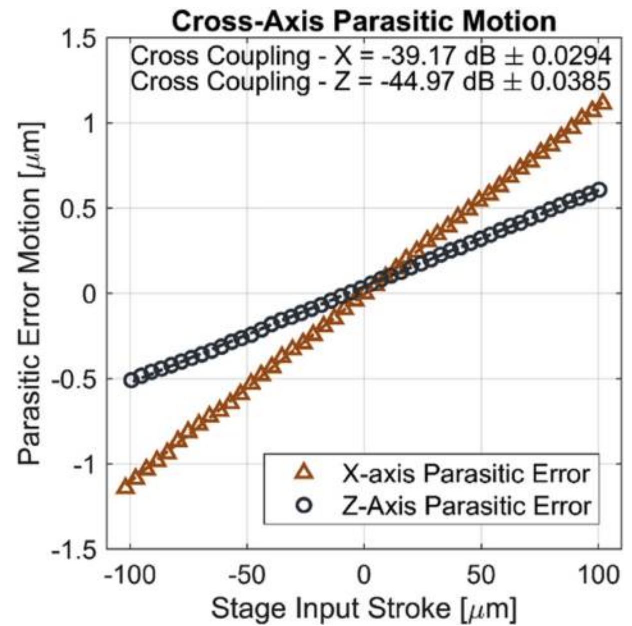

Fig. 9. Cross-axis parasitic error for both axis.

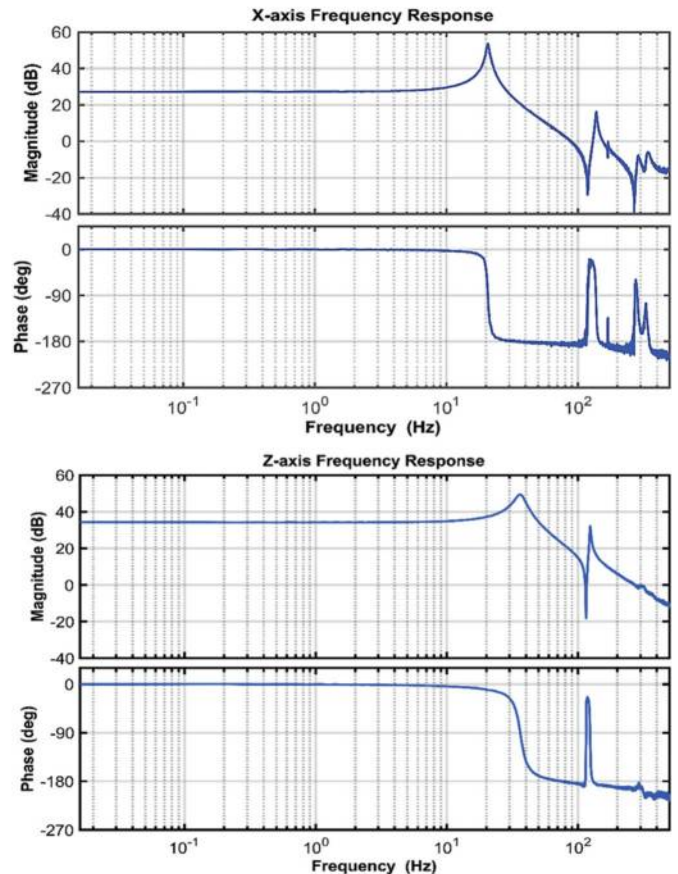

Fig. 10. Bode plots for both motion axis.

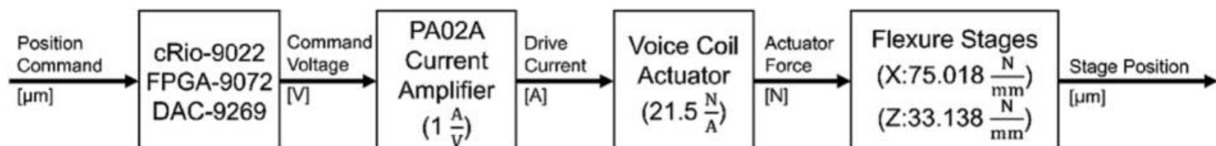

Fig. 8. System experimental apparatus block diagram.

ARTICLE IN PRESS

Table 2
Kerf corrected beam and FEA model, and experimental stiffnesses and first resonances.

Kerf Corrected Analytical		Kerf Corrected FEA		Experimental	
Parameter	Value	Parameter	Value	Parameter	Value
K_X	68.04 N/mm	K_X	74.01 N/mm	K_X	75.018 N/mm
K_Z	33.29 N/mm	K_Z	34.85 N/mm	K_Z	33.138 N/mm
First Mode X	23.6 Hz	First Mode X	24.6 Hz	First Mode X	20.83 Hz
First Mode Z	41.4 Hz	First Mode Z	42.4 Hz	First Mode Z	36.51 Hz

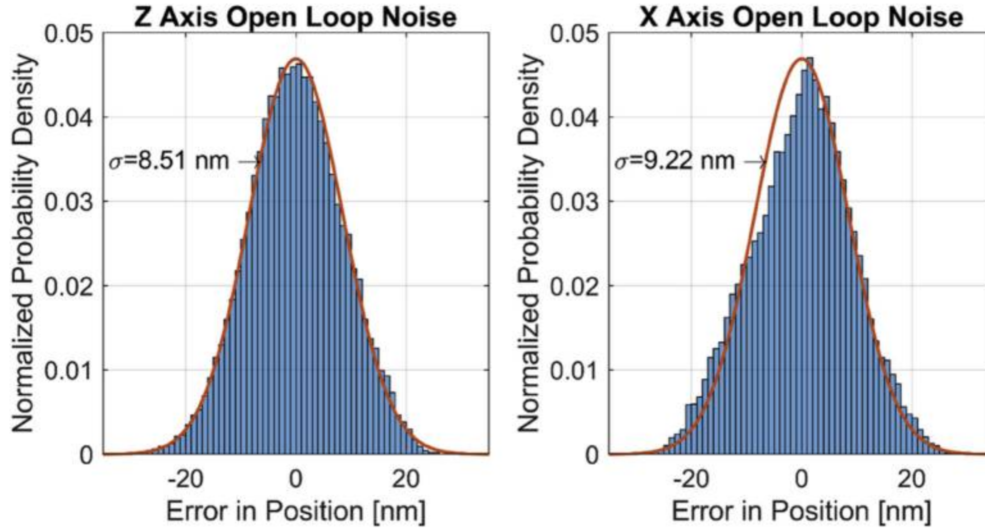

Fig. 11. Open Loop Noise Histograms Compared to Normal Distributions with the same mean and standard deviation for Both Motion Axis.

ability to meet modulus-to-yield strength ratio for the stated design range requirement and low cost, especially compared to 7000 series alloys with more optimal mechanical properties typically used in flexure stages [44].

2.2.2. sc-AFM approach mechanism and scanning

Final sample approach of the sc-AFM is accomplished through a small water-jet cut, 0.5 in thick 7075-T651 aluminum DPFM coupled to a 10 N voice coil actuator by a 4 inch slender rod (MotiCont LVCM 025-0-38-01) for a 200 µm maximum approach range as measured through finite element analysis (FEA) techniques. Al-7075 was used here as a small amount of free material was available, and the more favorable modulus-to-yield ratio allows for a higher maximum range. Design methodology of this flexure mechanism is detailed in previous work for wafer oriented in-line nanometrology [29]. The onboard sc-AFM piezoresistive sensor is used as sensor for approach feedback which allows the probe to quickly approach the sample to within scanning range without any destructive tip-sample contact. The probe tip is controlled for frequency modulation non-contact scanning of a 1 µm by 1 µm–20 µm by 20 µm area by a discrete PI controller (Atmel) and LabVIEW based software (ICSPI Corp.). The number of pixels per scan and tip dwell time at each point can be varied from 64 × 64 to 1024 × 1024 and from 200 µs to 2000 µs respectively through software to balance the tradeoff between scan speed and resolution and tailor tool operation to the exact critical dimension sensing required for any particular R2R nanomanufacturing process.

2.2.3. Gantry DPFM analytical model

The stiffness and maximum range of a double parallelogram flexure mechanism (DPFM) stage can be calculated from classical beam equations derived from first principles. Equations (2)–(5) were used to determine the beam thickness and DPFM width, height, and depth design parameters in order to meet the performance requirements enumerated for the large flexure monoliths where L, B, H and FOS represent the flexure beam length, plate depth, beam thickness, and factor of safety respectively [45,46]. Here k is used for stiffness and Disp_{Max} for maximum range for a given safety factor.

$$EI\ Y'' = M + FL \tag{2}$$

$$k_z = \frac{24EI_x}{L_x^3} \tag{3}$$

$$k_x = \frac{48EI_z}{L_z^3} \tag{4}$$

$$\text{Disp}_{\text{Max}} = \sigma_y * \frac{L^2}{3E * H * FOS} \tag{5}$$

The geometric parameters were chosen to balance the tradeoff between maximum range, DPFM stiffness, and moving mass capability. The 20 Hz or greater first resonant mode and mm retract range requirements were the primary constraints in the parametric mechanism design. The flexure dimensions chosen can be found in Table 1.

2.2.4. Finite element analysis

FEA studies were carried out in ANSYS 18 to aid in analyzing both the ideally-fabricated motion axis stiffnesses along with the critical first resonant mode of each axis of the DPFM monolith as various geometric parameters were altered. The FEA analysis was also used to confirm that the minimum factor of safety of maximum flexure beam von Mises stress at maximum actuation force with respect to 6061-T6 yield strength was adhered to. Fig. 5 shows the maximum single-sided displacement of each axis of the DPFM monoliths with the chosen actuator (68 N maximum force) also used to calculate mechanism stiffness. Further, the minimum FOS given the 68 N actuation force was found to be 7.44 in the X direction and 5.3 in the Z direction, both greater than the design minimum of 3. Stiffness results from FEA were also found to

ARTICLE IN PRESS

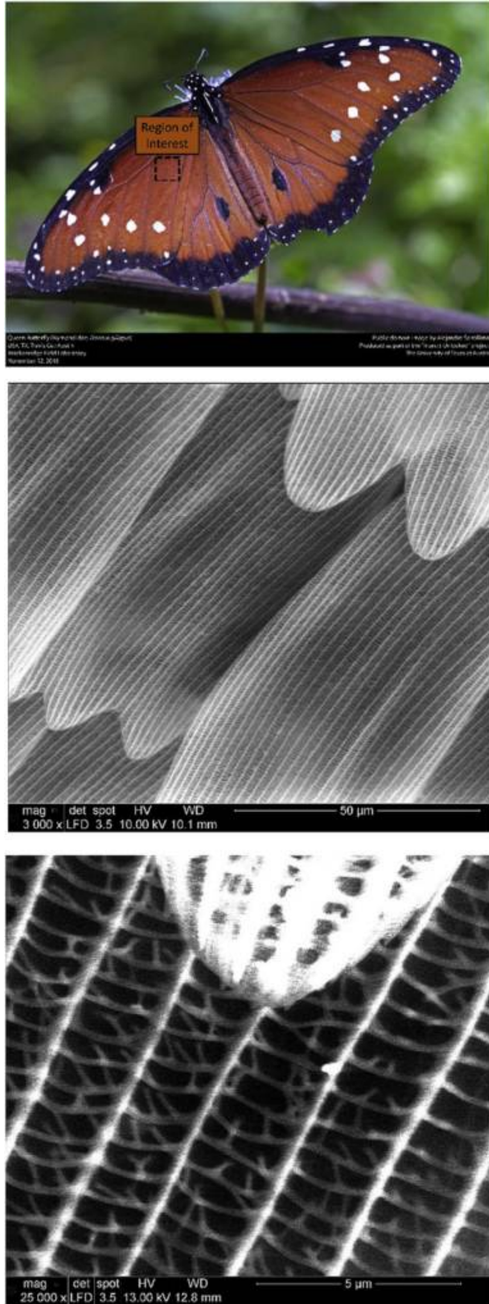

Fig. 12. (a) Photograph of queen butterfly (b) SEM image of hierarchical wing-scale microstructure (c) Zoomed SEM of wing nanostructure.

match analytical predictions within 10%. Lastly, a modal FEA study was conducted to ensure that the designed mechanism is able to meet the 20 Hz or greater first resonance mode requirement. As designed, the lowest first resonant mode found in the FEA study occurs in the X-axis mechanism at 21.2 Hz and the stiffness of the X and Z axis mechanisms were calculated as 50.2 N/mm and 34.2 N/mm respectively.

3. Gantry positioner fabrication

With design parameters set, the proof-of-concept tool was fabricated, and photographs of the setup with component overviews are shown in Fig. 6. In order to minimize the stiffness altering effects that AWJC kerf can cause, it was decided to cut two individual 0.5 in thick flexure plates per each individual DPFM monolith as opposed to a single 1 in thick flexure. The two 0.5 in flexure plates are then rigidly bolted to each other. Each plate is faced on both sides before AWJC, and, in an effort to minimize any sympathetic vibrations between the actual flexure beams which are not clamped between sides, a linear bearing grease is applied in between the inside faces of each flexure plate to provide viscous damping between flexure beams (Chicago Mfg. Extreme Pressure Lube #3). This helps to insure there is no sympathetic resonance or phase shift at higher order resonant frequencies between the two bolted plates in a single monolith. In order to account for the effect that the AWJC kerf will cause on the stiffness of the DPFM modules given the change in flexure beam stiffness, a correction factor is introduced to account for the effect in equations (7)–(10) where P, Q, B, and f_1 represent the top (during AWJC fabrication) flexure beam thickness, the larger bottom side beam thickness, the overall plate thickness, and first resonant mode respectively (see Fig. 7).

$$I_{yc} = B^*(P + Q)^*\frac{P^2 + Q^2}{48} \tag{7}$$

$$Correction\ factor\quad (Cf) = \frac{I_{trapezoidal}}{I_{rectangular}} \tag{8}$$

$$K_{corrected} = K_{rectangular}{}^*Cf \tag{9}$$

$$f_1^{kerf} = sqrt(Cf) * f_1 \tag{10}$$

In the particular case of the AWJC used, the water jet nozzle positioning system is rather inconsistent across its range, and the kerf on the cut flexure beams increases in overall taper (e.g. *P-Q*) the further away from the center of the plate the cut is made and the lower the magnitude of the AWJ nozzle velocity vector. This causes variation in kerf at corners and where the path of the AWJ nozzle turns sharply or reverses. Thus, an average of several measurements of overall taper across the length of the DPFM flexure beams was used to calculate the correction factor for each respective mechanism, found to be 1.476 for the X-axis mechanism and 1.018 for the Z-axis mechanism.

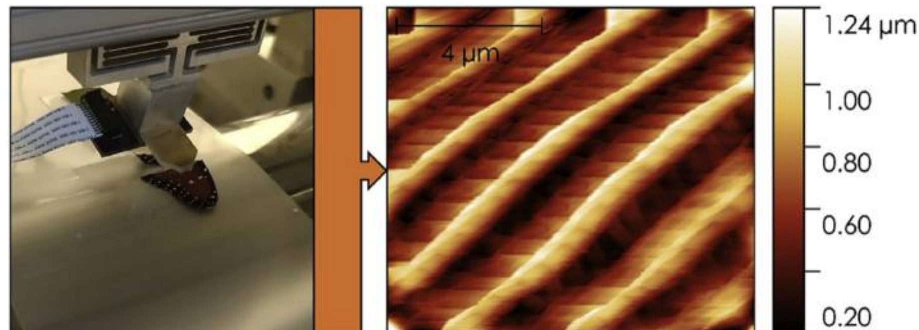

Fig. 13. In-line sc-AFM Scan of Queen Butterfly Wing on Polycarbonate Substrate.

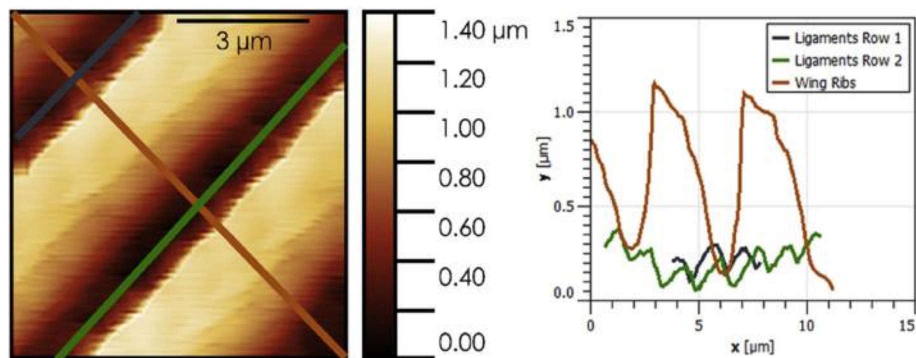

Fig. 14. 33.7 s Scan of Queen Butterfly Wing and Metrology Data.

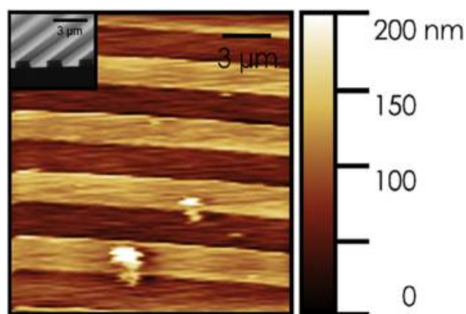

Fig. 15. 31.9 s AFM Scan of TGZ2 Calibration Grating Attached to the Polycarbonate Web (Ted Pella Inc.).

4. Experimental results

The proof of concept tool was tested in order to evaluate the performance of the critical nanopositioning system along with the tool as a whole. Capacitance probes measuring the position of the motion stage in each axis to an accuracy of 2 nm at 10 kHz were utilized (LION Precision, CPL290, NI-9239). The voice coil actuators (MotiCont LVCM-051-064-02) were driven by a current amplifier and digital-to-analog converter (Apex Microtechnology PA02A, NI-9269). A block diagram detailing the DC gains and actuation flow of the various components of the experimental system is shown in Fig. 8.

4.1. Gantry flexure mechanism stiffness and parasitic motion

Inputs spanning the range of the capacitance sensors utilized for measurement (200 µm) at 0.5 Hz, 4 µm steps were recorded along with the parasitic motion of the non-actuated axis during each test to calculate as-fabricated stiffnesses and the parasitic motion ratio of both motion axis. Fig. 9 details the parasitic motion behavior of the stage. The stiffness of the X and Z axis respectively was calculated from fitting a Hooke's law linear curve to the actuated stage displacement with respect to stage input force. As-fabricated stiffness was found to be 75.018 N/mm and 33.138 N/mm respectively. Both of these values are within 5% of the expected stiffness from the FEA study with kerf correction. Moreover, as it is more challenging to design a high-performance control system for a multiple-input multiple-out (MIMO) system like the two axis DPFM modules if the level of cross-coupling between axis is high, it is desirable for this parasitic motion to be minimized when actuating the opposite axis bearing. Generally, if cross-coupling is below – 30 dB each two-axis flexure monolith can be considered as if it were two independent single-input single-output (SISO) systems [47]. This cross-coupling gain, essentially the parasitic:desired motion ratio, was found to be −39.17 dB and −44.97 dB for the X and Z DPFM axis respectively. Thus, each monolith degree of freedom may be viewed as a SISO systems for future closed-loop control implementation in the experimental setup – this vastly simplifies application of advanced control techniques [48].

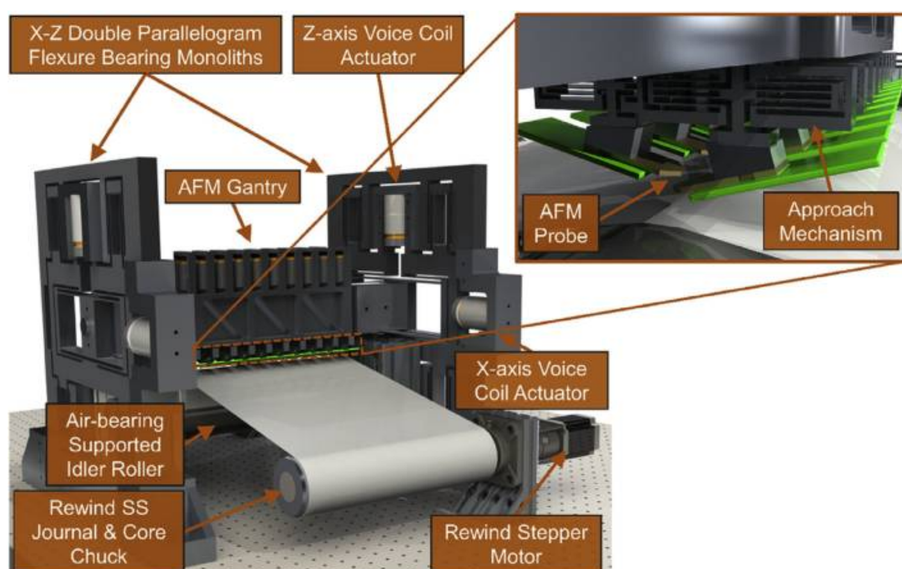

Fig. 16. Render of future multi-probe metrology tool.

ARTICLE IN PRESS

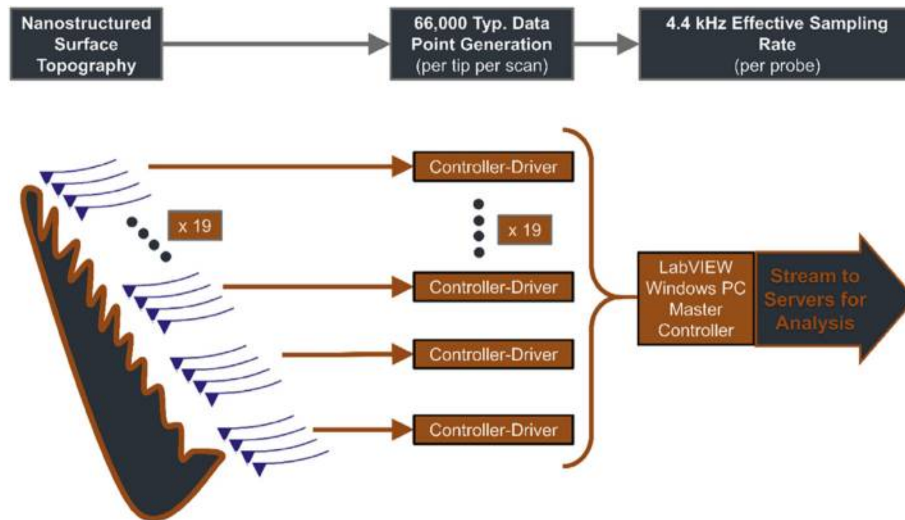

Fig. 17. Proposed multi-site inspection data flow.

4.2. Gantry nanopositioner frequency response and open loop performance

To collect frequency response data in order to evaluate as-fabricated resonance modes of the DPFM modules, a 1000 Hz gaussian white noise signal was outputted to the voice coil current amplifiers and the stage response recorded with capacitance sensors. From this data, Bode plots of both the X- and Z-axis open loop response are generated and are shown in Fig. 10 [49]. The X-axis shows an experimental first resonant peak of 20.82 Hz, within about 15% of the kerf-corrected value expected from the previous FEA study. The Z-axis, experimentally found to be 36.51 Hz, falls in the same range with about a 14% variation from the expected, kerf-corrected FEA value found with Eq. (10). Both of these variations are considered within the acceptable range for modal FEA studies [49,50]. Comparison of the kerf-corrected beam model, FEA study, and experimental stiffness and first resonance values is shown in Table 2. Higher, out-of-plane and uncontrollable resonance modes of the DPFM "wings" (i.e. secondary grounds) all fall above 120 Hz, and exact shapes and frequencies can be found in the supplemental information section of this paper.

The AFM gantry positioning system was then operated in open-loop mode at a constant command and its noise in position measured at 10 kHz sampling. A low noise floor was a design goal of the nanopositioners, and a key driver of the > 20 Hz first resonant mode requirement. Upon evaluation, the X-axis was found to have a 1-σ deviation of 9.22 nm and the Z-axis 8.51 nm – both of which are within the sub-10 nm design requirement (Fig. 11). Open-loop control is thus adequate for stop-and-scan operation of the prototype tool.

4.3. Tool metrology performance

Flexible, nanofeatured test or calibration artifacts with critical dimensions suited to the capabilities of the sc-AFM can be very costly. Instead, the wing of a Queen Butterfly is chosen for its nanoscale features and representative structure applicable to many hierarchical and photonic materials [51,52]. Furthermore, the structure of the individual scales is an excellent test case due to the presence of both μm-scale wing "ribs" and nm-scale wing "ligaments" connecting the ribs making up the porous, multi-scale structure of the wing scales. Fig. 12 shows a photograph and two SEM images with increasing levels of magnification to provide a baseline with which to compare the in-line sc-AFM data. A photograph of the test scanning condition and the post processed AFM scan showing the nanostructure of a single scale on the butterfly wing demonstrates the capability of the proof-of-concept tool and can be seen in Fig. 13. Moreover, a ∼30 s scan of the same nanostructure is shown along with nanometrology data derived from the scan in Fig. 14. This illustrates the high-speed scanning capability while retaining nm-scale tip height resolution and resolution flexibility of the tool. Slower, more detailed scans can be taken when more information is necessary, otherwise fast ∼30 s scans are default. To fit within the 60 s JFIL step-and-print time budget, 5 s are allotted to probe approach & retract, 34 s to sc-AFM scanning, < 1 s to gantry positioning, and up to 20 s for web movement and time for air damping to decay any unwanted web disturbances or vibrations after each step-and-scan cycle.

Further, to ensure fidelity of data taken with the sc-AFM, a scan of a 92.5 ± 3 nm step height by 3 μm period silicon precision calibration grating attached to the 150 μm thick, 80 mm wide polycarbonate web was carried out using the proof-of-concept tool. Average scan time for the probe settings used to acquire the data shown in Fig. 15 was found to be 31.9 s. For this scan, X and Y pixel sizes are calculated to be 117 nm and 132 nm respectively given total scan area and number of pixels where tip data is recorded. From post-processing, the calculation of average step height and standard deviation of the grating found experimentally with the tool is 93.9 ± 2.9 nm [53]. This agreement with the calibration grating manufacturer specification provides validation to the flexible-substrate data captured with the prototype tool.

5. Conclusion and future work

A novel framework for tip-based process feedback in R2R nanomanufacturing is presented and the design of a proof-of-concept tool for high-speed metrology of nanoscale features on a flexible substrate inline with R2R manufacturing was detailed, fabricated, and demonstrated, be it for eventual use with photonic films, energy- or metamaterials, or flexible hybrid electronics. Unlike wavelength-limited or indirect optical or IR based measurement methods, or time-consuming and costly electron beam inspection, the nanometrology system presented herein can achieve the high scan speeds, nanometer-scale resolution, and uniquely compact in-line packaging necessary to optimize and implement real time process feedback in the ever-challenging environment of R2R nanofabrication. Moreover, sc-AFM scans of a Queen Butterfly's wing microstructure and a 92.5 nm step height by 3 μm period calibration grating, all attached to a 150 μm thick polycarbonate web, were conducted. Average time for the scan settings utilized in maximal speed scans with sub 150 nm lateral pixel sizing was shown to be under 34s.

In order to fully realize the potential for this process control methodology in future work, the number of sc-AFM probes and approach mechanisms will be scaled to proportionally increase overall

ARTICLE IN PRESS

throughput of the metrology tool (Fig. 16). Due to the advantageous modularity of the sc-AFMs and their discrete controller-drivers, there is no addition computational cost to increasing the number of probes implemented in a specific design. Furthermore, improved versions of the probes themselves utilizing four cantilevers packaged on each single chip have been demonstrated, this quadruples the amount of nanometrology data which can be collected per cycle [28]. Given the 350 mm wide web the tool is designed for, the number of sc-AFMs can be scaled to 19, and thus the number of active scanning cantilevers to 76. This improves potential metrology data throughput for the proposed tool from 400 μm^2/min to 0.0608 mm^2/min, or an effective per-probe data sampling rate of 4.4 kHz for 256 × 256 px scans (Fig. 17). As a modern semiconductor foundry may have upwards of 50,000 sensors sampling at over 1 kHz, the throughput of the proposed parallel measurement methodology is well within current data infrastructure capabilities. Furthermore, at current costing for single cantilever probes, this pluralized metrology approach would only represent a roughly $4000 expenditure for 19, a worthwhile capital cost increase with respect to the rough yearly costs publicly available from NIST for 2015, $153 million, and any potential cost decreases a R2R fab with true in-line nanometrology capability might experience [7].

Declaration of interest

The authors have no conflicts of interest to report.

Acknowledgements

The authors would like to thank Dr. Nilabh Roy, Martin Ward, James Garcia, Mikaela Wilson and Dr. Richard Piner for the many helpful and informative discussions and the ICSPI Corp. for their valuable advice and material support. This research is based upon work supported primarily by the National Science Foundation under Cooperative Agreement No. EEC-1160494 and by the National Science Foundation Graduate Research Fellowship program under Grant No. 2017251210.

Appendix A. Supplementary data

Supplementary data to this article can be found online at https://doi.org/10.1016/j.precisioneng.2019.04.001.

References

[1] UNESCO and ITU. The state of broadband 2018: broadband catalyzing sustainable development. International Telecommunication Union; 2018.
[2] Nathan A, et al. Flexible electronics: the next ubiquitous platform. Proc IEEE 2012;100(SPL content):1486–517.
[3] U.S. Department of Energy. Roll to roll processing. Innov Clean Energy Technol Adv Manuf 2015;34.
[4] Bauer S. Flexible electronics: sophisticated skin. Nat Mater 2013;12(10):871–2.
[5] Hong S, Myung S. Nanotube Electronics: a flexible approach to mobility. Nat Nanotechnol 2007;2(4):207–8.
[6] Park S, Vosguerichian M, Bao Z. A review of fabrication and applications of carbon nanotube film-based flexible electronics. Nanoscale 2013;5(5):1727–52.
[7] O'Connor AC, Beaulieu TJ, Rothrock GD. Economic analysis of Technology infrastructure needs for advanced manufacturing: roll-to-roll manufacturing. 2016.
[8] Subbaraman H, Lin X, Xu X, Dodabalapur A, Guo LJ, Chen RT. "Metrology and Instrumentation challenges with high-rate, roll-to-roll manufacturing of flexible electronic systems. Instrum. Metrol Stand Nanomanufact, Opt Semicond VI 2012;8466:846603.
[9] Vaid A, et al. In-line E-beam wafer metrology and defect inspection: the end of an era for image-based critical dimensional metrology? New life for defect inspection. Metrol Insp Process Control Microlithogr XXVII 2013;8681:86810D.
[10] Singh V, Bosman SJ, Schneider BH, Blanter YM, Castellanos-Gomez A, Steele GA. Optomechanical coupling between a multilayer graphene mechanical resonator and a superconducting microwave cavity. Nat Nanotechnol Aug. 2014;9:820.
[11] Urbach HP, Pereira SF, Ushakova K, Roy S, van den Berg Q. Radially polarized light for detection and nanolocalization of dielectric particles on a planar substrate. Phys Rev Lett 2015;114(10):1–5.
[12] Roy S, Pereira SF, Urbach HP, Wei X, El Gawhary O. Exploiting evanescent-wave amplification for subwavelength low-contrast particle detection. Phys Rev A 2017;96(1).
[13] Kirchner G, et al. Toward high volume solution based roll-to-roll processing of OLEDs. J Mater Res 2017;32(12):2219–29.
[14] Zhu R, et al. Scatterometry for nanoimprint lithography. J Vac Sci Technol B, Nanotechnol Microelectron Mater Process Meas Phenom 2016;34(6):06K503.
[15] Logothetidis S, Georgiou D, Laskarakis A, Koidis C, Kalfagiannis N. In-line spectroscopic ellipsometry for the monitoring of the optical properties and quality of roll-to-roll printed nanolayers for organic photovoltaics. Sol Energy Mater Sol Cells 2013;112:144–56.
[16] Zenyuk IV, Englund N, Bender G, Weber AZ, Ulsh M. Reactive impinging-flow technique for polymer-electrolyte-fuel-cell electrode-defect detection. J Power Sources 2016;332:372–82.
[17] Ulsh M, Porter JM, Bittinat DC, Bender G. Defect detection in fuel cell gas diffusion electrodes using Infrared thermography. Fuel Cells 2016;16(2):170–8.
[18] Kreuzer M, Whitworth GL, Francone A, Gomis-Bresco J, Kehagias N, Sotomayor-Torres CM. In-line metrology for roll-to-roll UV assisted nanoimprint lithography using diffractometry. Apl Mater 2018;6(5):0–6.
[19] Muhamedsalih H, Blunt L, Martin H, Hamersma I. An integrated opto-mechanical measurement system for in-process defect measurement on a roll-to-roll process. Laser Metrol Mach Perform XI, Lamdamap 2015 2015:99–107.
[20] Blunt L, Fleeming L, Elrawemi M, Robbins D, Muhamedsalih H. In-line metrology for defect assessment on large area roll to roll substrates. 11th laser metrol. Precis. Meas. Insp. ind. 2014. May, 2014.
[21] Gao F, et al. In-situ defect detection systems for R2R flexible pv barrier films. In ASPE 2015 summer topical meeting. 2013.
[22] Dai G, Koenders L, Fluegge J, Hemmleb M. Fast and accurate: high-speed metrological large-range AFM for surface and nanometrology. Meas Sci Technol 2018;29(5):11–5.
[23] ICSPI Corporation. nGauge atomic force microscope. 2018.
[24] Strathearn D, Sarkar N, Lee G, Olfat M, Mansour RR. The benefits of miniaturization of an atomic force microscope. Proc IEEE Int Conf Micro Electro Mech Syst 2017:1363–6.
[25] Sarkar N, Lee G, Mansour RR. CMOS-MEMS dynamic FM atomic force microscope. Transducers 2013;2013(June):916–9.
[26] Sarkar N, Strathearn D, Lee G, Olfat M, Mansour RR. A platform technology for metrology, manipulation & automation at the nanoscale. Int. Conf. Manip. Autom. Robot. Small scales, MARSS 2017 - proc. 2017.
[27] Sarkar N, Strathearn D, Lee G, Olfat M, Mansour RR. A 0.25mm^3 atomic force microscope on-a-chip. 2015 28th IEEE int. Conf. Micro electro mech. Syst. 2015. p. 732–5.
[28] Olfat M, Strathearn D, Lee G, Sarkar N, Hung SC, Mansour RR. A single-chip scanning probe microscope array. Proceedings of the IEEE international conference on micro electro mechanical systems (MEMS). 2017. p. 1212–5.
[29] Yao T-F, Duenner A, Cullinan M. In-line metrology of nanoscale features in semiconductor manufacturing systems. Precis Eng 2016;47:147–57.
[30] NanoSystem-solutions, "D-light DL-1000 maskless photolithography system". 2012. no. Datasheet.
[31] Neutronix-quintel, "NXQ9000 roll-to-roll photolithography". 2018. p. 95037. no. 408.
[32] Lim H, et al. Roll-to-roll nanoimprint lithography for patterning on a large-area substrate roll. Microelectron Eng 2014;123:18–22.
[33] John J, Tang Y, Rothstein JP, Watkins JJ, Carter KR. Large-area, continuous roll-to-roll nanoimprinting with PFPE composite molds. Nanotechnology 2013;24(50).
[34] Smolka M, et al. Roll-to-Roll pilot line for large-scale manufacturing of microfluidic devices. 2017.
[35] V Sreenivasan SV. Nanoimprint lithography steppers for volume fabrication of leading-edge semiconductor integrated circuits. Microsyst Nanoeng 2017;3(April):17075.
[36] Ahn S, et al. Roll-to-roll nanopatterning using jet and flash imprint lithography. 2012;8323. 83231L–8323–7.
[37] Ahn SH, et al. High-performance wire-grid polarizers using jet and Flash™ imprint lithography. J Nanolithogr MEMS, MOEMS Aug. 2013;12(3):031104.
[38] Carter Kenneth. R2R nanofabrication: a test bed platform for UMass nanoscale science technologies. 2011.
[39] Lan H. Large-Area nanoimprint lithography and applications. Micro/nanolithogr - Heuristic asp Endur Technol 2018.
[40] Kim M, et al. Antireflective, self-cleaning and protective film by continuous sputtering of a plasma polymer on inorganic multilayer for perovskite solar cells application. Sol Energy Mater Sol Cells 2019;191(October 2018):55–61.
[41] Sajid M, Dang HW, Na KH, Choi KH. Highly stable flex sensors fabricated through mass production roll-to-roll micro-gravure printing system. Sens Actuators A Phys 2015;236:73–81.
[42] Zhou X, Xu H, Cheng J, Zhao N, Chen S-C. Flexure-based roll-to-roll platform: a practical solution for realizing large-area microcontact printing. Sci Rep 2015;5(April):10402.
[43] Choi K, Zubair M, Ponniah G. Web tension control of multispan roll-to-roll system by artificial neural networks for printed electronics. Proc Inst Mech Eng Part C J Mech Eng Sci 2013;227(10):2361–76.
[44] Awtar S, Parmar G. "Design of a large range XY nanopositioning system. Vol. 2 34th annu. Mech. Robot. Conf. Parts A B, vol. 5. 2013. p. 387–99. May 2013.
[45] Li C, Wang J, Chen SC. Flexure-based dynamic-tunable five-axis nanopositioner for parallel nanomanufacturing. Precis Eng 2016;45:423–34.
[46] Zhou X, Wang D, Wang J, Chen SC. Precision design and control of a flexure-based roll-to-roll printing system. Precis Eng 2015;45:332–41.
[47] Maroufi M, Moheimani SOR. Cross coupling in parallel kinematic MEMS nanopositioners. Proceedings of the ASME 2015 dynamic systems and control conference

ARTICLE IN PRESS

2016. V003T52A006.
[48] Yong YK, Liu K, Moheimani SOR. Reducing cross-coupling in a compliant XY nanopositioner for fast and accurate raster scanning. IEEE Trans Control Syst Technol 2010;18(5):1172–9.
[49] Roy NK, Cullinan MA. Fast trajectory tracking of a flexure-based, multiaxis nanopositioner with 50-mm travel. IEEE/ASME Trans Mechatron Dec. 2018;23(6):2805–13.
[50] Roy N, Cullinan M. Design of a flexure based XY precision nanopositioner with a two inch travel range for micro-scale selective laser sintering. Proc. Annu. Meet. Am. Soc. Precis. Eng. 31st annu. Meet. 2016. p. 1–2.
[51] Dallaeva D, Tomanek P. AFM study of structure influence on butterfly wings coloration. Adv Electr Electron Eng 2012;10(2):120–4.
[52] Zhang W, Gu J, Liu Q, Su H, Fan T, Zhang D. Butterfly effects: novel functional materials inspired from the wings scales. Phys Chem Chem Phys 2014;16(37):19767–80.
[53] Nečas D, Klapetek P. Gwyddion: an open-source software for SPM data analysis. Cent Eur J Phys 2012;10(1):181–8.